ADVANCED ENERGY & SUSTAINABILITY RESEARCH
www.advenergysustres.com

Recent Advances in Surface Functionalized 3D Electrocatalyst for Water Splitting

Nadira Meethale Palakkool, Mike P. C. Taverne, Owen Bell, Jonathan D. Mar, Vincent Barrioz, Yongtao Qu, Chung-Che Huang,* and Ying-Lung Daniel Ho**

Hydrogen is gaining attention as a fossil fuel alternative due to its potential to meet global energy demands. Producing hydrogen from water splitting is promising as a clean and sustainable fuel pathway. The hydrogen evolution reaction (HER) and oxygen evolution reaction (OER) are crucial in electrocatalytic water splitting for energy conversion and storage. However, water electrolysis faces challenges in cost, efficiency, and scalability. Alternative transition metal electrocatalysts and emerging 2D materials advance electrolysis research, though transitioning from academia to industry remains challenging. The introduction of 3D-printing technologies has revolutionized electrode fabrication for HER and OER. This review explores integrating 3D-printing technologies and surface functionalization with non-noble metal-based electrocatalysts and emerging 2D materials. It focuses on surface-functionalized 3D-printed electrodes using technologies like selective laser melting, stereolithography, and fused deposition modeling with non-noble metal electrocatalysts such as transition metal oxides, hydroxides, and emerging 2D materials like transition metal carbide/nitride (MXenes) and transition metal dichalcogenides (TMDCs). The review highlights the opportunities and challenges in scalable fabrication, long-term durability, and cost-efficiency for practical implementation. Future research directions include exploring new materials for 3D printing and alternative electrocatalysts alongside leveraging theoretical and machine-learning approaches to accelerate the development of competitive materials for water electrolysis.

1. Introduction

Even though hydrogen is commonly recognized as the next-generation fuel and is being extensively studied, the uneconomical production cost and practical inapplicability of hydrogen-generating systems restrict it to mostly laboratory-scale applications.[1,2] Electrocatalytic water splitting is a promising but still-in-development approach to resolve the energy crisis by generating clean or green hydrogen.[3,4] Among the various energy conversion systems, it is widely recognized as the ideal method for generating carbon-free and high-energy hydrogen fuel with no bespoken contamination.[5–8] Electrocatalytic water spitting involves two significant steps: hydrogen evolution reaction (HER) and oxygen evolution reaction (OER).[9] The former refers to reducing water to molecular hydrogen at the cathode and the latter the oxidation of water to oxygen at the anode.[10] Commercial catalysts based on platinum are widely used for hydrogen production due to their superior catalytic activity and stability.[11] Platinum while highly effective, is notably expensive (992 $ per ounce) and very rare with a crustal abundance of only 37 parts per billion.[12] Given the typical loading requirement for effective catalysis, high cost hinders feasible commercialization of Pt-based electrocatalysts.[13] In the realm of OER, iridium oxide (IrO_2) and ruthenium oxide (RuO_2) are considered the benchmark electrocatalysts due to their excellent activity and relatively high conductivity of 104 $cm^{-1}\,\Omega^{-1}$.[14–17] IrO_2 is the best-known OER catalyst in acidic media due to good activity and stability.[17] However, it is costly, priced at $500 per ounce, and is one of the scarcest elements with abundance less than 10% that of Pt.[14] Besides, RuO_2 also serve as the most active electrocatalyst for

N. Meethale Palakkool, M. P. C. Taverne, O. Bell, V. Barrioz, Y. Qu, Y.-L. D. Ho
Department of Mathematics, Physics & Electrical Engineering
Northumbria University
Newcastle upon Tyne NE1 8ST, UK
E-mail: y.qu@northumbria.ac.uk; daniel.ho@northumbria.ac.uk

The ORCID identification number(s) for the author(s) of this article can be found under https://doi.org/10.1002/aesr.202400258.

DOI: 10.1002/aesr.202400258

J. D. Mar
School of Mathematics, Statistics and Physics
Newcastle University
Newcastle upon Tyne NE1 7RU, UK

C.-C. Huang
Optoelectronics Research Centre
University of Southampton
Southampton SO17 1BJ, UK
E-mail: cch@soton.ac.uk

OER.[18] Especially, (RuO_2) based materials have emerged as appealing catalysts due to their competitive price (42 $ per ounce) much lower than Pt and (IrO_2).[19] However, they are less stable and tend to oxidize to RuO_4 under high anodic conditions.[20] In this regard, enormous research has been undertaken for developing alternative noble-metal-free electrocatalysts for OER and HER including first-row transition metals, and their derivatives such as oxides, hydroxides, and chalcogenides.[21–28] However, due to their inherently lower intrinsic catalytic activity, these materials require high catalytic surface loading, which results in a lack of long-range order control and diminished charge transfer efficiency.[29,30] Additionally, most of them endure inefficient conductivity and stability.[31] To develop highly efficient noble-metal alternatives, electrocatalysts with unique electronic structures and tuneable morphology have been developed.[32] This includes various emerging two-dimensional (2D) materials such as transition metal dichalcogenides (TMDCs) and transition metal carbides/nitrides (Mxenes).[33–39] However, the conventional transfer processes for functionalizing these materials have adverse effects, such as the depletion of active sites by the destruction of their intrinsic structures.[40]

Recently, 3D printing or additive manufacturing technologies have evolved as a convertible and customizable platform for designing and fabricating 3D-structured materials for various applications including electrochemistry.[41–45] 3D printing involves the layer-by-layer fabrication of computer-aided predesigned structures.[46] The freedom in design and the wide range of material options have enabled this technology to demonstrate significant advancements in recent studies.[47] 3D printing simplifies the manufacturing process in several ways. First, it reduces costs by minimizing material waste, as it only requires the amount of material needed to create each product. Second, it decreases the need for extensive supply chains and transportation, as products can be printed on-site, reducing carbon emissions. Additionally, 3D printing enables more efficient and customizable production, potentially reducing energy consumption. These advantages lead to a reduced carbon footprint, making 3D printing a more sustainable and eco-friendly technology.[48] While 3D-printing offers a straightforward approach for designing components like electrodes, as discussed in this review, it is essential to acknowledge that, this technique can be applied to fabricate all cell components for electrolyser.[7,49–51] As highlighted in a recent study by Lee et al. despite the advantages of 3D printing for proof-of-concept and foundational research, it may present further challenges in scaling up and achieving broader adoption of this technology.[52] However, it is anticipated that 3D printing will complement traditional fabrication methods rather than replace them entirely. Moreover, 3D printing enables automated processes, ensuring uniformity between batches by eliminating variations that can arise from manual intervention, leading to more consistent and reliable production. This is critical in bridging the gap between prototyping and large-scale industrial production.[53]

3D-printed electrodes have intricate designs and large controllability over hierarchical porous structures, which enhances the performance of OER and HER reactions.[54–56] Since the intrinsic activity of a catalyst depends on its atomic and electronic structure, it is imperative to obtain high current densities in water splitting.[57] With its precise control over electrode configuration and hierarchical porous channels, 3D printing enables the efficient use of geometric surface area and exposed active sites in electrocatalysts, optimizing the reaction energy barrier.[58,59] The high surface area of the 3D-printed electrodes provides a larger electrode/electrolyte interface and high sensitivity, enhancing the electrochemical performance.[60] However, many of the 3D printable materials studied so far including stainless steel,[61] graphene[62] and polymer[49] could not accomplish the desired electrochemical properties. Their performance is limited by factors such as lower corrosion resistance and impaired charge transfer capabilities, resulting in a lack of inherent electrocatalytic properties.[63–66] The recent trend in electrochemistry follows the combination of different materials and fabrication strategies for synergistically improving the characteristics of materials whilst reducing cost.[67–69] Researchers have developed ongoing interest in modifying the 3D-printed electrode surfaces for different electrochemical applications.[61,70,71] Surface functionalization, the added dimension toward practical applications, can overcome the intrinsic limitations of available 3D printable materials by combining inexpensive materials and advanced equipment.[72] To date, studies have been conducted with various 3D-printing techniques combined with simple to complex surface modification strategies from atomic layer deposition (ALD) to commercial spray coating.[46,73,74] As illustrated in **Figure 1**, integration of 3D-printing with surface functionalization can greatly alleviate major bottlenecks of electrocatalyst fabrication, addressing challenges related to the fabrication process and electrochemical performance. The surface functionalization of the 3D-printed electrodes outperforms conventional noble-metal electrocatalysts (Figure 1a) by optimizing the use of non-noble metal counterparts such as transition metal compounds and emerging 2D materials. This is achieved by the design freedom of 3D printing, allowing high mass loading of the transition metal-based catalysts without sacrificing efficiency, overcoming the typical limitation associated with mass loading on conventional substrates (Figure 1b). Additionally, the emerging 2D electrocatalysts can be integrated with 3D-printed electrodes by avoiding costly and complex transfer processes, and optimizing these materials within their structure (Figure 1c). The surface functionalization of 3D-printed electrodes overcomes inherent limitations such as insufficient catalytic activity, low conductivity and stability, often limiting the electrocatalytic activity (Figure 1d). Hence, the combination of 3D-printing with non-noble metal and 2D-materials-based electrocatalysts surpasses the limitations of their unmodified counterparts and usage of conventional substrate-based synthesis (Figure 1e).

Considering the rapid advance and new achievements in the integration of 3D printing and noble-metal-free materials for hydrogen generation from electrocatalytic water splitting, there is a need for a detailed and critical review to fully understand and further motivate research. Various literature has been dedicated to reviewing the progress and development of electrocatalytic water electrolysers based on 3D-printed electrodes.[75–79] To the best of our knowledge, numerous reviews have been presented discussing the surface modification of 3D-printed materials for different applications.[80–83] However, there are no dedicated reviews for surface-modified 3D-printed electrodes

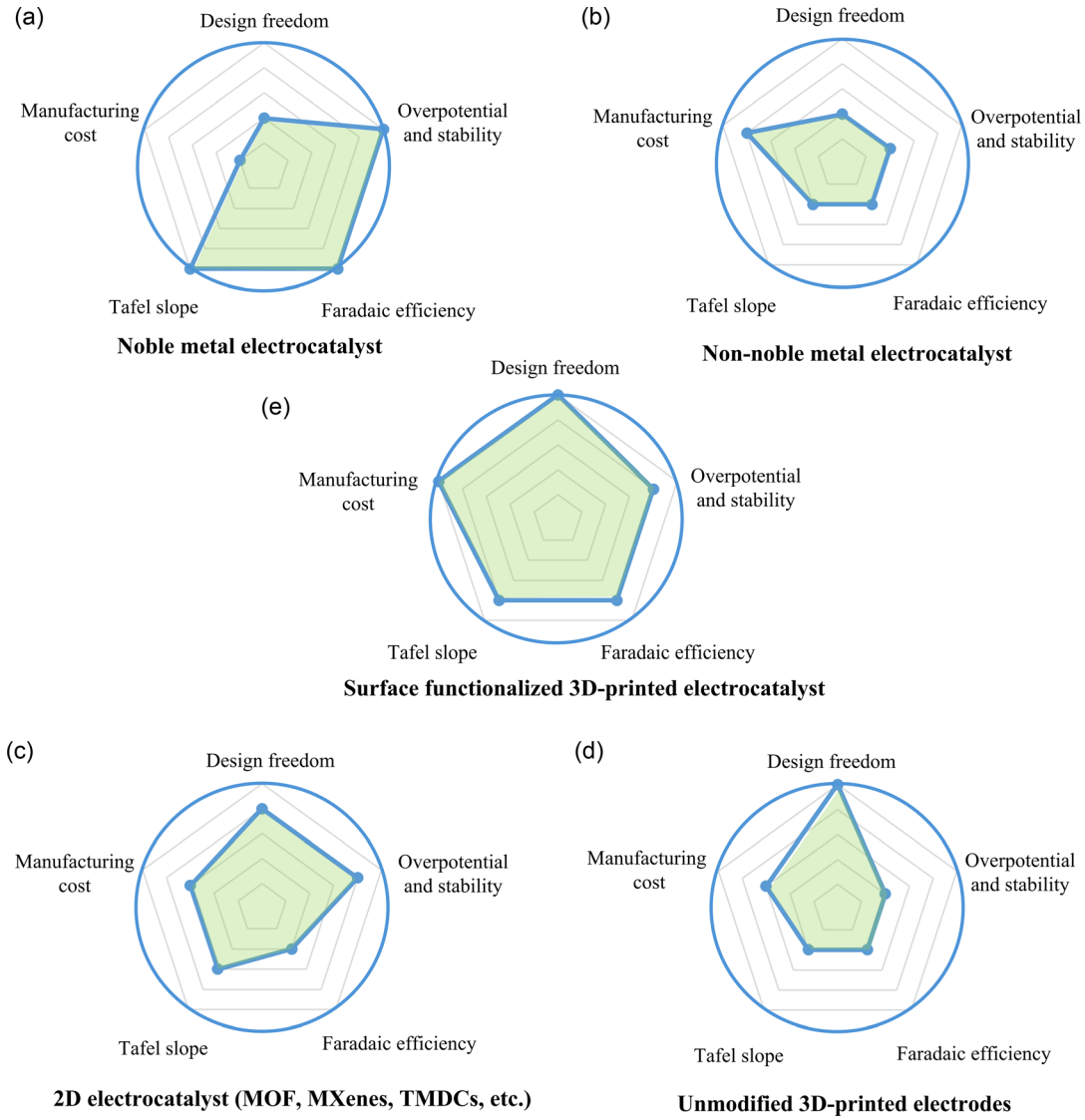

Figure 1. Radar chart illustrating the prospects of combining 3D-printing and surface functionalization. a) Noble metal electrocatalyst. b) Non-noble metal electrocatalyst. c) Surface functionalized 3D-printed electrocatalyst. d) 2D electrocatalyst (MOF, MXenes, TMDCs, etc.). d) Unmodified 3D-printed electrodes.

for water-splitting reactions. Herein, we reviewed the recent advances in the development of 3D-printed electrocatalysts modified using various non-noble metal active materials. In the following sections, we will first explore the fundamentals of water splitting and the principles of 3D printing. We will then discuss fabrication methods and performance of electrocatalysts for HER, OER, and overall water-splitting applications.

2. Electrocatalytic Water Splitting—Overview

Electrochemical water splitting is a prominent strategy to produce hydrogen to replace non-renewable fossil fuels.[84] Hydrogen with about 99.999 vol% can be obtained with this technique, with consequent drying of the produced hydrogen and removing dissolved oxygen.[85] However, hydrogen generated from water splitting has only engaged around 4% of the global hydrogen industry.[86] This emphasizes the timeliness to accelerate hydrogen production efficiency and reduce associated production costs.[87]

The water-splitting reaction consists of two half-reactions, namely HER and OER. The half-reactions take place through the mechanisms depending on the electrolyte environment:[88]

1) In acidic solution

Cathode

$$2H^+ + 2e^- \rightarrow H_2 \quad (1)$$

Anode

$$H_2O \rightarrow \frac{1}{2}O_2 + 2H^+ + 2e^- \quad (2)$$

2) In neutral solution
Cathode

$$2H_2O + 2e^- \rightarrow H_2 + 2OH^- \quad (3)$$

Anode

$$H_2O \rightarrow \frac{1}{2}O_2 + 2H^+ + 2e^- \quad (4)$$

3) In alkaline solution
Cathode

$$2H_2O + 2e^- \rightarrow H_2 + 2OH^- \quad (5)$$

Anode

$$2OH^- \rightarrow H_2O + \frac{1}{2}O_2 + 2e^- \quad (6)$$

A thermodynamic potential of 1.23 V is required for electrochemical water splitting under standard conditions, corresponding to an energy input of $\Delta G = 237.1\ kJ\ mol^{-1}$.[89] However, it has been widely identified that the slowness of OER can critically diminish the electrochemical efficiency of the overall water-splitting reaction, irrespective of the electrolyte medium.[90] This is due to the greater number of electron transfer reactions in the OER, unlike single-step cathodic reactions, and the need to apply a higher potential than the theoretical cell voltage to overcome the kinetic barrier.[41,59,60] The extra electrical energy necessary to overcome the intrinsic activation barrier of the electrocatalysts is referred to as overpotential (η). In addition to kinetic limitations, factors such as the interfacial resistance between the electrode and electrolyte also lead to a voltage drop. Consequently, the practical voltage $E_{practical}$ of the overall water-splitting cell will be higher than the thermodynamic potential and can be elucidated as

$$E_{practical} = 1.23V + \eta_{anode} + \eta_{cathode} + \eta_{other} \quad (7)$$

where η_{anode} and $\eta_{cathode}$ represents the kinetic overpotentials of anode and cathode, respectively, and η_{other} represents additional overpotential.

Conventionally, the overpotential required to obtain a current density of 10 mA cm^{-2} is the determining parameter for comparing the activity of electrocatalysts. This current density value is equivalent to the 12.3% efficiency of solar water-splitting devices.[91] As evident from Equation (7), reducing the overpotential is of paramount importance to accomplish efficient water splitting. This is to say, the kinetic overpotentials can be reduced by increasing electrocatalyst activity, while electrolyser design can be refined to lower the interfacial resistance and corresponding overpotential.[84] While the overpotential of electrocatalysts provides kinetic information, the free energy of gas adsorption (ΔG) involving both HER and OER gives insights into thermodynamic information regarding reaction intermediates and the electrocatalysts.[10,84] An ideal electrocatalyst should achieve a nearly zero ΔG with suitable surface and interfacial properties. Additionally, Tafel polarization analysis offers important insights into the reaction kinetics of the electrocatalyst, as well as the corrosion properties of coated materials.[54] The Tafel slope and exchange current density are other important kinetic parameters obtained from the Tafel equation.

$$\eta = a + b \log j \quad (8)$$

where η, b, j, and a denote the overpotential, Tafel slope and current density of the respective electrocatalyst and the intercept of Tafel plot, respectively. Due to their optimal binding energy and Gibb's free energy for gas adsorption, noble metals such as Pt, Ir, and Ru and their oxides are considered ideal electrocatalysts for HER and OER.[92,93] Despite the ability of noble metals to accomplish the existing electrochemical and energy demands, their high production cost and scarcity stand out as critical barriers to economic viability.

3. 3D-Printing Technologies

The 3D-printing or additive manufacturing technology denoted the nature of the process, involving layer-by-layer fabrication of 3D parts is maturing into a powerful manufacturing strategy. Characterized by their advantages and disadvantages, different methods of 3D-printing fabrications have been classified based on the raw materials and manufacturing techniques. Among the various 3D-printing techniques, only a few methods can produce conductive electrodes and substrates. This includes fused deposition modeling (FDM) using conductive carbon filaments, selective laser melting (SLM) using metallic powders and direct ink writing (DIW) using conductive ink. However, current literature has explored the integration of surface functionalization and 3D-printing techniques limited to a few of them. **Table 1** summarizes the overview of different 3D-printing techniques, comparing the advantages, disadvantages, materials used, and printing resolution.

3.1. Fused Deposition Modeling

The FDM represents the most common extrusion-based 3D printing established by Scott Crump, the co-founder of Stratasys, in 1989.[94] In this process, a thermoplastic filament is extruded via a high-temperature nozzle typically kept at temperatures up to 200 °C.[95] It primarily involves acrylonitrile butadiene styrene (ABS), polylactic acid (PLA), and polycarbonate (PC) as the precursor materials.[96] Despite the various advantages of polymers such as low cost and versatile processibility, these materials lack functionality and mechanical strength. Recently, polymers reinforced with fillers such as ceramic, metal, and wood fiber have been shown to compensate for the poor mechanical stability of the polymer in 3D-printed components.[97] This technique is known for its cost-effectiveness and ability to result in durable and mechanically resistant 3D-printed parts and components. The major limitations of FDM 3D printing are low printing precision, increased building time, poor surface texture, and the inability to produce highly complex 3D structures.[94] A study by Quero et al. reported the effect of the geometry of printer parts, such as the nozzle, in enhancing the quality of 3D printing resolution.[98] This study helps to address traditional limitations associated with FDM printing, such as lower accuracy and less-refined surface texture.

Table 1. Comparison of different 3D-printing technologies: advantages, disadvantages, materials used and the resolution.

3D printing technique	Materials	Advantages	Disadvantages	Resolution
Fused deposition modeling (FDM)	Thermo-plastic polymer	Inexpensive, easy processing, non-toxic and inflammable material, wider material choice	Low resolution, limited to simple geometric designs, poor surface finishing	0.02–0.1 mm[172]
Direct ink writing (DIW)	Polymers, hydrogels and ceramics	High resolution, inexpensive, no need for support, multi-material processibility, low-temperature processing	Post-processing requirement, lower mechanical strength, slower processing, environmental sensitivity	0.1 mm to several millimeters[173]
Stereolithography (SLA)	Photo-curable resin	High accuracy and resolution, functional prototyping, smooth surface finish, reasonably fast, complex and intricate geometric designs	Need for support structure, high maintenance cost, toxic precursor material, limited material choice, requires complex post-processing	0.025–0.3 mm[102]
Selective laser melting (SLM)	Powders of metal and alloys	Flexible material selection, complex geometric designs, high accuracy, functional integration	Post-processing requirements, costly equipment and material, limited build volume	0.03–0.1 mm[174]

3.2. Direct Ink Writing

Direct ink writing, also known as robocasting, is an extrusion-based 3D printing technique that operates by precisely depositing precursor material in a controlled manner. This technique robotically operates by a stage moving in three axes, extruding the precursor ink via a micronozzle in a layer-wise manner.[99] Materials ranging from polymers, ceramics, plastics, and different composite materials are used to fabricate complex 3D structures. This type of 3D printing allows the fabrication of 3D structures with resolutions ranging from microns to submicrons range. The ink composition and 3D printing parameters can be tailored to produce 3D structures with optimal features. The major challenge of this technique lies in the preparation of ink as its viscosity and concentration determine the ability of the 3D structure to retain its shape after deposition.[100] Another limitation is the necessity of post-modification procedures such as sintering or drying to improve the mechanical properties.[96]

3.3. Stereolithography

Stereolithography (SLA) is an established 3D-printing technique developed by Chuck Hull in 1986.[101] Besides, he developed the STL file format as part of their commercial 3D printer. The format represents the digital model of the 3D object which can be transferred to the 3D printer. This technique involves applying ultraviolet (UV), visible, infrared, or laser to create well-defined 3D structures for various applications. It produces multi-layer structures from light-sensitive resins which solidify when exposed to the light.[96] These resins consist of monomers and suitable photoinitiators, which activate the photopolymerization process. Exposure to light enables the monomers to cohere with each other and form solid parts in a layer-by-layer manner. Unlike extrusion-based 3D-printing techniques, SLA is characterized by high printing resolutions.[102] However, material compatibility is a concern limited to only photosensitive materials, which can be cured by light or laser.[103] Typically, acrylate and epoxy-based resins are used as precursors for stereolithography. These materials do not have inherent electrochemical properties and often require post-processing or co-mixing with conductive materials. Despite offering high precision and resolution, this technique can lead to longer processing time and increased cost, potentially impacting its feasibility for large-scale applications.[104]

3.4. Selective Laser Melting

Selective laser melting (SLM) is a subset of the powder bed fusion technologies used in metal 3D printing. This technique works on the principle of high-temperature melting of spread layers of powdered precursor bed into the desired 3D component.[83] The most common precursor materials used in SLM are stainless steel, nickel, titanium, and precious metal alloys.[105] As the SLM produces conductive metallic parts, surface modification can be easily performed to enhance the desired electrochemical functionalities.[42] SLM offers key advantages, including high flexibility in structural design and enhanced mechanical properties and density of 3D-printed parts compared to traditional manufacturing methods.[106] However, this technique often results in rough surfaces, necessitating additional surface smoothening procedures. Further disadvantages are the need for support structures and the high cost associated with the energy-demanding process.

4. Surface Functionalized 3D-Printed Electrodes

The mass activity of the electrocatalyst is dependent on the electrochemical active surface area per loaded mass and specific activity.[107] Studies have shown that improving the surface area by high mass loading or refining catalyst morphology to enhance the exposed surface area can partially overcome these limitations.[59] High mass loading on conventional substrates can diminish the mass activity during electrolysis by blocking active sites and preventing effective gas transport.[55] The introduction of 3D supports such as nickel and copper foams has partially mitigated this issue.[108–111] These are considered 3D porous electrodes that allow the hydroxyl ions and gases to cross through, which are proven to show high intrinsic activity as they speed up oxygen bubble transport through the enhanced surface

area.[112,113] However, these materials lack industrial feasibility due to template demand, costly subtractive manufacturing technologies, and poor geometry control.[6] Furthermore, the random porous structure results in significant bubble trapping thereby increasing the ohmic resistance and restraining practical energy efficiency.[114] The ongoing interest in 3D-printing technologies is to incorporate suitable active materials on hierarchically porous electrodes by tailoring aspects such as geometry, exposed surface area, and mass transfer channels.[107] 3D printing can control the geometric structure, feature size, interconnectedness, and uniformity of electrodes. This allows the study of various electrocatalytic materials with precisely engineered 3D electrodes as a supporting platform.[55] The following discussion emphasizes the diverse applications of 3D-printed electrode surfaces functionalized with different non-noble metal electrocatalytic materials. 3D printing paves a novel way for the fabrication of complex 3D structures of long-range order that are difficult to obtain from conventional methods. **Figure 2** summarizes the various techniques and materials used for 3D printing and surface functionalization to fabricate electrodes for OER and HER applications. The following subsections discuss recent progress in and challenges of integration of 3D printing and noble-metal free-surface functionalization for electrocatalytic water-splitting reactions.

4.1. Surface Functionalized 3D-Printed Electrodes for HER

4.1.1. Transition Metal Dichalcogenides

Transition metal dichalcogenides (TMDs) have gained relevance as HER catalysts due to their low cost and high chemical stability.[24] MoS_2 represents the 2D layered TMDs formed by a layer of Mo atoms sandwiched by two layers of S atoms.

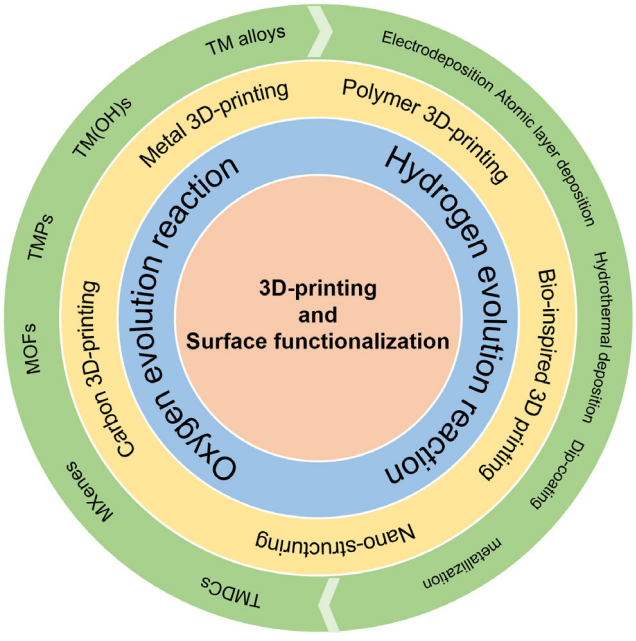

Figure 2. Electrocatalyst fabrication approaches by combining 3D-printing and surface functionalization.

Multi-layered MoS_2 is commonly composed of different polymorphic structures. The most common polymorphs are tetrahedral, hexagonal, octahedral, and rhombohedral symmetries denoted as 1 T, 2 H, and 3 R, respectively, where digits represent the number of crystallographic layers in the unit cell.[115] MoS_2 contains Mo edge active sites and unsaturated S vacancy sites, making it suitable for electrocatalytic applications.[36] However, poor conductivity and constricted edge sites often restrict the electrocatalytic activity of bulk MoS_2.[116] Various transfer techniques have been employed to extract mono/few layers of MoS_2.[117] Herein, we discuss the various efforts to combine 3D printing with MoS_2 modification for HER applications.

Recently Urbanová et al. explored the combination of 3D-printing and ALD for fabricating electrocatalysts for HER application.[73] In this work, the titanium-based substrate for the electrode was 3D-printed and subsequently modified with MoS_2 as represented in **Figure 3**a. ALD is an emerging technique used to produce thin film materials with atomic-scale precision for various applications including electrochemical energy storage and conversions.[118] As ALD involves a volatile gaseous precursor that thermally reacts and deposits on the surface of the substrate only, the physical and chemical properties of the precursor play a crucial role.[119] Utilizing the high surface area of the 3D-printed electrode, electrocatalytic properties of MoS_2 with different layer thicknesses were studied. Furthermore, this work provided insights into the important role of the number of cycles of ALD in tailoring the thickness and surface morphology of the electrode and therefore the HER activity. Among different electrodes modified, MoS_2 obtained with 125 cycles of ALD displayed excellent HER performance with an overpotential of −0.4 V and Tafel slope of 56 mV dec $^{-1}$ (Figure 3b). These values are superior to the unmodified and spray-coated sample electrodes prepared in this study. Furthermore, it was found that there was no significant change in electrochemical performance for samples deposited with more than 125 ALD cycles. The Raman spectra of the optimized sample exhibited peaks corresponding to three main characteristic vibrational modes of the trigonal prismatic (2H) phase of MoS_2. It was concluded that the materials showed superior stability over 250 catalytic cycles. This study emphasizes the vital role of 3D-printed surfaces to improve the deposition of catalytic materials via complex processes such as ALD to obtain superior electrocatalytic performance. Nevertheless, the scaling up of MoS_2 production via ALD remains relatively challenging due to the high cost and complexity of the process.[120] Potentially reduced conductivity and material compatibility of 3D printed materials for thermal conditions are also challenges that can impact performance and durability.[121]

In that respect, various studies have suggested that MoS_2 can be deposited on 3D-printed electrodes in facile and cost-effective techniques without compromising the excellent electrochemical properties of the material. Rui et al. modified a 3D-printed carbon electrode alongside other substrates with MoS_2 in a timesaving approach involving commercial spray coating.[74] The 3D-printed electrode made from graphene and PLA filaments was solvent-activated with dimethylformamide (DMF) before spray coating of MoS_2. The solvent activation resulted in the effective dissolution of the insulating polymer filament

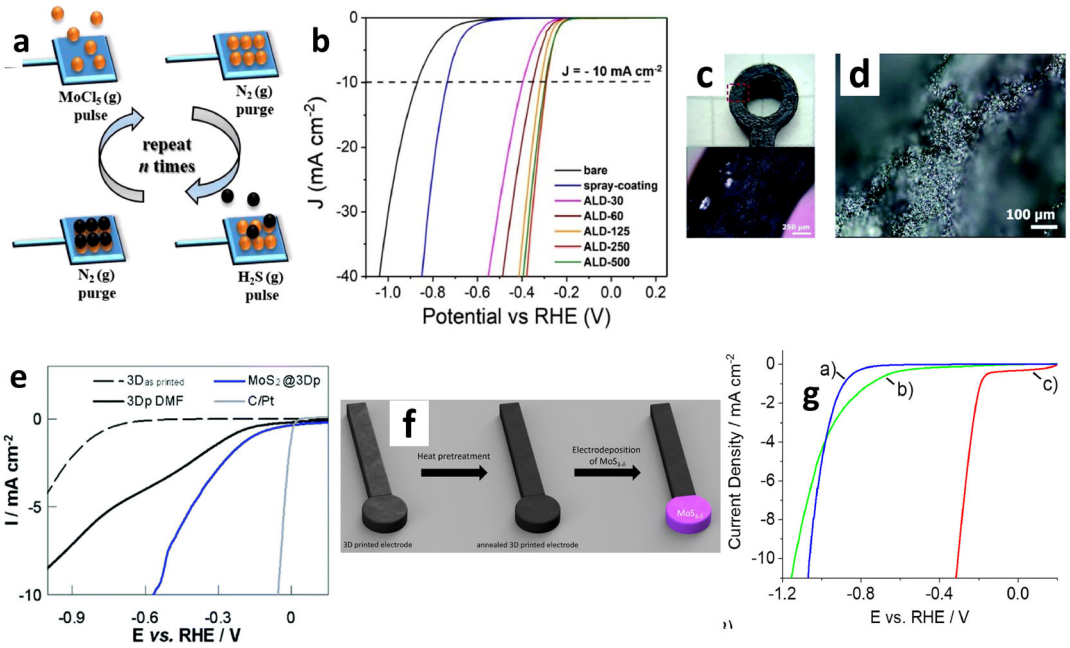

Figure 3. a) Schematic representation of atomic layer deposition of MoS_2 on 3D-printed Ti substrate. b) Polarization curves of bare, spray-coated and ALD-modified 3D electrodes in 0.5 M H_2SO_4. Reproduced with permission.[73] Copyright 2021, Elsevier Ltd. c,d) Optical images of a 3D printed electrode modified with MoS_2 by spray coating. e) LSV curves of the 3D printed electrodes in 0.5 M H_2SO_4. Reproduced with permission.[74] Copyright 2019, The Royal Society of Chemistry. f) Schematic illustration of 3D electrode surface modified via electrodeposition. g) Polarization curves of the glassy carbon (a), annealed 3D-printed electrode (c) and MoS_2 modified 3D-printed electrode. Reproduced with permission.[122] Copyright 2020, Elsevier Ltd.

and hence an increase in electrocatalytic activity. Figure 3c shows an optical image of an MoS_2-modified 3D electrode. The electrode thus obtained not only exhibited uniform distribution in the top plane of the electrode but also the lateral interior walls (see Figure 3d). The 3D-printed electrode modified by spray coating of MoS_2 exhibited an improved HER performance with an overpotential of 560 mV significantly better than the as-printed 3D electrode with an overpotential of 470 mV to obtain a current density of 10 mA cm^{-2} (Figure 3e). The XPS data revealed that the dried film of MoS_2 obtained from commercial spray constitutes 1T and 2H phases along with oxidized species. According to the authors, the hindrance of oxidized species in the electrocatalytic performance will be compensated by the presence of 1H phases. Additionally, the electrode showed stability over 2 h −550 mV versus RHE. However, when combining spray coating and complex 3D-printed geometries, achieving the same consistency and uniform coverage might not be possible, leading to inconsistent catalytic performance. In addition, Iffelsberger et al. (2020) presented a facile surface modification of MoS_2 via electrodeposition.[122] The self-standing 3D-printed electrodes were prepared from PLA/graphene filament and modified with MoS_2 through electrochemical deposition. The 3D-printed electrode was pre-treated via thermal annealing to remove the contents of PLA. Figure 3f represents the schematic illustration of the fabrication process. Primarily, the catalytic activity of the electrocatalyst was analyzed via linear sweep voltammetry (LSV). The transition metal dichalcogenide-modified 3D printed electrode exhibited a significantly lower overpotential of -0.297 ± 0.016 V—superior to the unmodified electrode with −1.14 V (Figure 3g). Furthermore, the Tafel slope of the electrode was revealed to be −119 mV dec^{-1}. The material was further characterized with scanning electrochemical microscopy to substantiate the electrochemical analysis. This analysis revealed the heterogenic surface catalytic activity, given the importance of localized activities of HER within the high surface area of the electrodeposited electrode. Precise control of catalyst loading and layer thickness using electrodeposition offers significant benefits, allowing customized 3D designs to achieve improved performance. However, this precision poses challenges, as optimizing these conditions for complex geometries may require considerable effort and experimentation to achieve consistent results.[123]

4.1.2. MXenes

MXenes are a novel family of two-dimensional (2D) inorganic compounds discovered by Yuri Gogotsi's research group in 2011.[124] These 2D compounds constitute transition metal carbides and nitrides as atomic layers with the general formula $M_{n+1}X_nT_x$, where M represents early transition metals such as titanium, vanadium, or molybdenum, X stands for carbon and/or nitrogen, T denotes the surface termination which includes groups like —OH, —O and —F, and $n = 1$, 2 or 3.[125] Following its discovery, various kinds of MXenes have been synthesized, studied using computational methods and used for various applications due to their excellent structural and chemical stability, superior electrical conductivity, and improved active surface area.[126–128] MXenes are gaining significant attention

in various electrochemical applications due to their high electronic conductivity and hydrophilicity.[129–131]

Recently, conventional carbon materials have been replaced by 3D-printed carbon for electrochemical applications. Despite the development of numerous carbon-based porous electrodes, HER catalyst materials tend to be adherent to the surface of the porous structure thus limiting the utility of interconnected porous surfaces.[132] On the other hand, bare 3D-printed carbon electrodes suffer from poor electrochemical performance. Studies have shown that materials such as MXenes can be used to modify the 3D-printed carbon electrode. Akshay Kumar et al. demonstrated a prototype of 3D-printed nanocarbon electrodes dip-coated with MXene ($Ti_3C_2T_x$) with catalytic activity toward HER.[133] The 3D electrode designed using Autodesk Fusion 360 software was printed using fused deposition modeling (FDM) 3D printing. The 3D-printed electrode was modified via binder-free dip coating in a slurry of MXene ($Ti_3C_2T_x$) (**Figure 4**a). SEM imaging revealed that the titanium carbide layers are attached to the 3D-carbon surface. Elemental composition study via EDS analysis substantiates this with the additional presence of F and O which the author ascribed as the consequence of surface termination. The as-prepared electrode attained a current density of 200 mA g^{-1} at a potential of −0.481 V and Tafel slope 335 mV dec^{-1} (Figure 4b). Unlike complex methods such as ALD, dip-coating provides a more straightforward material deposition technique. This method alleviates the requirement of complex precursor handling and intricate procedural control, making it an accessible alternative for various applications.[134,135] However, this is often limited to simple geometries, and careful optimization is required to achieve consistent coverage on complex structures. Moreover, there is a lack of understanding of interactions between the electrode surface and 2D catalyst materials. Integrating theoretical studies helps to address this challenge and provides valuable insights on catalyst design and fabrication.[136]

4.1.3. Transition Metal Alloys

Besides modifications using a single transition metal, many studies have reported the combination of two or more transition metals (alloys) resulting in considerable improvement in conductivity and overpotential reduction in HER performance. In a work by Hüner and coworkers, a 3D-printed graphene-based electrode coated with nickel and cobalt alloys was studied for HER activity in an alkaline medium. The 3D electrode was prepared using conductive PLA filament via the Ultimaker 3D printer as depicted in Figure 4c.[137] The coating process involved an electrochemical deposition by applying a constant voltage of 10 V for 1 h. Ni and Co were deposited at different composition ratios and the sample with Ni–Co ratio corresponding to 1:4 presented superior activity over other samples at a current density of 10 mA cm^{-2} (Figure 4d). The varying composition of metal has affected the grain size of the deposit, as confirmed by SEM and electrochemical impedance spectroscopy (EIS) analyses. Besides, in another

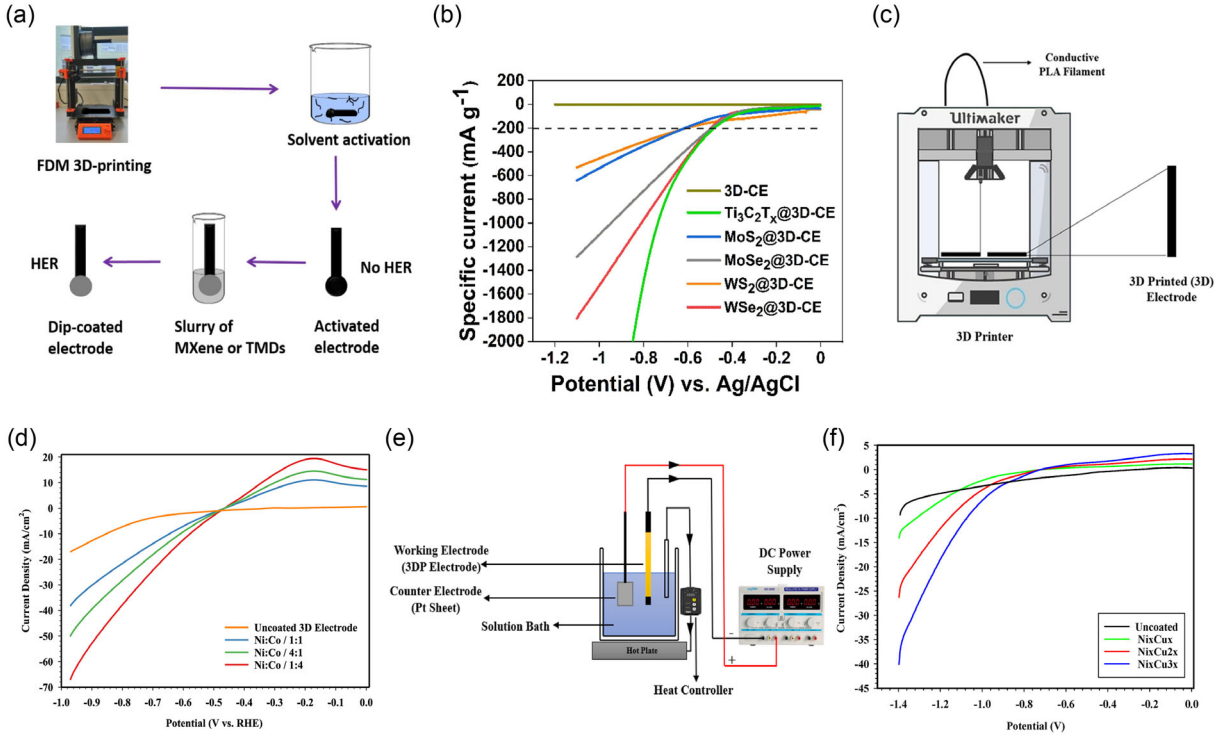

Figure 4. a) Illustration of dip-coating procedure of the activated 3D-printed nanocarbon electrode. b) LSV measurement of different electrodes prepared by dip-coating. Reproduced with permission.[133] Copyright 2021, Elsevier Ltd. c) Schematic illustration of 3D printing process using Ultimaker 3D printer. d) LSV curves of 3D electrodes modified with different compositions of Ni-Co. Reproduced with permission under the terms of the CC-BY 4.0 license.[137] Copyright 2023, The Authors. Published by the American Chemical Society. e) Representation of electrodeposition process. f) Polarization curves of different electrodes modified with Ni–Cu. Reproduced with permission.[138] Copyright 2022, Elsevier Ltd.

study by the same authors, a PLA-based electrode was deposited with different volume ratios of Ni and Cu.[138] The fabrication process was followed by a similar method using conductive PLA filament. The 3D electrodes were modified with NiCu alloys of varying compositions via electrochemical deposition. The metal compositions were found to affect surface morphology thereby the electrochemical performance. Figure 4e represents the illustration of the electrodeposition process involved in the study. The grain size of the deposit and the roughness of the surface were affected by the varying concentrations of metals. Furthermore, the electrode modified with a 1:3 ratio of NiCu achieved a current density of 40.12 mA cm^{-2} at −1.4 V in an alkaline medium. This was confirmed with EIS analysis, revealing a lower resistance value of the optimized electrode. Both studies show the versatility of the modification process for tailoring electrode activity and kinetic performance, although optimization requires considerable time and effort.

4.2. Surface Functionalized 3D-Printed Electrodes for OER

Some studies have focused on optimizing the extrinsic properties of electrocatalysts such as surface area, mass transport, and wettability of 3D-printed electrodes.[6,62,139] These investigations demonstrate that electrode synthesis by precisely controlling these properties can result in high-performance materials. This is particularly important for OER as it involves multielectron transport processes and the formation of reactive oxygen intermediates.[90] Hence the intricate mechanism of OER requires effective mass transport and readily accessible active sites on the catalyst surface so that the intermediates can be efficiently produced and removed.[140]

4.2.1. Transition Metal Chalcogenides

Transition metal chalcogenides have also been studied for OER applications. For example, Chang et al. prepared 3D-printed hierarchical support with 3D microarchitectures from stainless steel and modified with $NiCo_2S_4$ nanoneedle catalyst via hydrothermal method.[55] The 3D printing technologies provide freedom over the controllability of printable designs. In this respect, the authors of this work demonstrated a pattern of metal supports with porous and hollow structures (see **Figure 5**a). The electrode support with the optimized geometry showed enhanced electrolyte infiltration and reduced capillary effect of the hollow structure. As can be seen in Figure 5b, this electrode support modified with $NiCo_2S_4$ nanoneedle exhibited an OER performance with an overpotential of 226 mV, at a current density 10 mA cm^{-2}. This is attributed to increased electrochemical active surface area (ESCA) as confirmed by the analysis of electrochemical double-layer capacitance from cyclic voltammetry (CV) measurement. While hydrothermal synthesis allows precise control over reaction conditions that synthesize material with tailored properties, issues associated with expensive metal hardware such as autoclaves remain challenging. Additionally, the fixed volume of

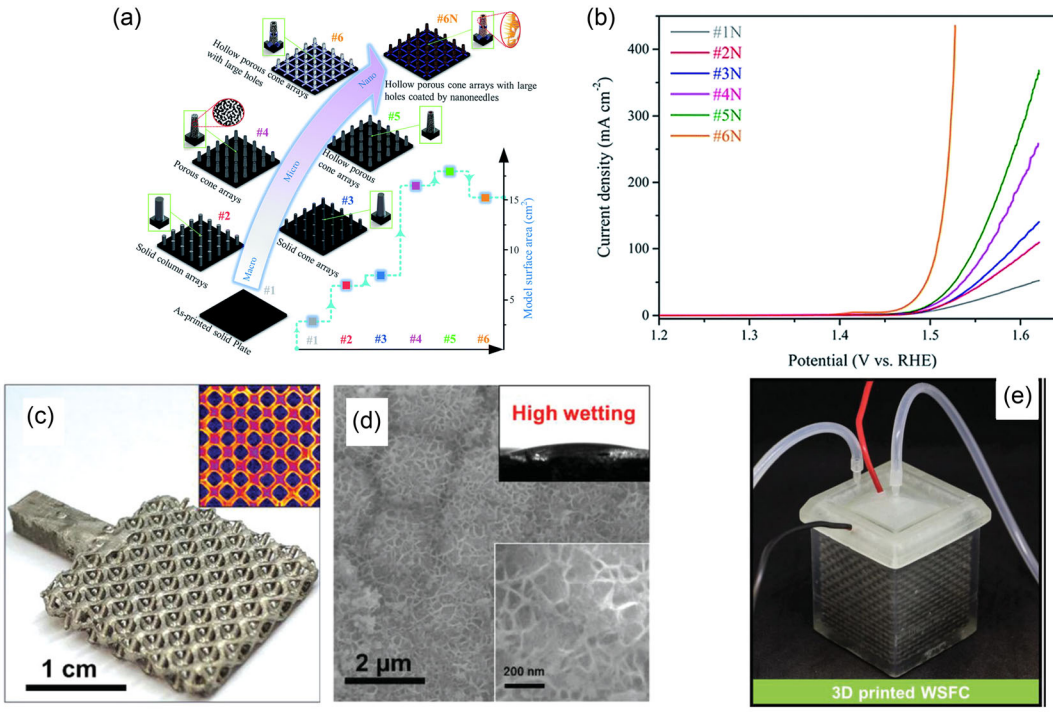

Figure 5. a) Different structure models designed for the electrode support using CAD software. b) Comparison of LSV curves of samples prepared using various electrode supports at a scan rate of 1 mV s^{-1}. Reproduced with permission.[55] Copyright 2019, The Royal Society of Chemistry. c) Digital image of the Ni–P electrode obtained using computer tomography. d) The SEM image of the electrode indicates the honeycomb structure and the high wettability. e) Water-splitting full cell assembled using the 3D-printed electrodes, electric wires, and pipes. Reproduced with permission under the terms of CC-BY 4.0.[49] Copyright 2019, The Authors. Published by Wiley-VCH.

traditional reactors restricts fabrication to small scales and inhibits its scale-up considerations.[141]

4.2.2. Transition Metal Phosphides

Besides chalcogenides, transition metal phosphides (TMPs) are another class of material well-known for catalyzing OER, owing to their hexagonal crystal structure suitable for high conductive surfaces.[142] 3D printing enables the fabrication of polymer structures via different available techniques. However, its application in electrochemical devices is limited by electrical conductivity, as studies conducted so far have not explored conducting polymers. As a viable solution, researchers are exploring various possibilities for modifying the polymeric structure via different electrochemical techniques. For example, Xinran Su and coworkers reported the fabrication of an octa-truss structured polymer substrate via SLA 3D printing and its subsequent metallization.[49] The modification process involved an electroless deposition of a NiP conductive layer followed by the electrodeposition of Ni nanosheets. Figure 5c represents the digital image of the NiP-plated sample and the computer tomography, and 5 d the SEM image of a honeycomb-like structure. Further, the authors developed a water-splitting full cell using the metalized polymer electrode along with other 3D-printed components including a semi-permeable gas bubble separator and gas collection guide (Figure 5e). The 3D polymer/NiP/NiFe-nanosheet electrode exhibited a bifunctional electrocatalytic activity in a basic medium, with an OER overpotential of 197 mV at a current density of 10 mA cm^{-2}. Further, this study has shown that the conductivity of the polymer can be greatly increased with an effective conductivity of 4.7×10^4 S m^{-1} after metallization, which surpassed the conductivity of previously reported conductive polymeric structures.

With the rise of 3D printing technologies, researchers are exploring the expansive possibilities of bioinspired materials. In this respect, Peng et al. investigated the 3D printing of graphene-based electrodes incorporated with ID carbon nanotubes (ID CNT) for overall water splitting application.[62] 3D-printed graphene electrodes have been known to possess elastic and compression-resistant properties but with poor flexibility. Herein, the electrode design was inspired by the geometry of the 1D setae of the gecko's feet. Like the rows of setae of gecko's feet that can adequately adhere to the vertical glass, the electrode nanostructure was designed as graphene interlaced with 1D CNT to oppose the bending force that arises from surface tension and buoyancy when immersing in water (See SEM images in **Figure 6**a,b). The electrodes were prepared via extrusion-based 3D printing using mixed ink of partially reduced graphene oxide and CNTs. The electrode shows a tensile stress of 96.2 kPa while studied as a function of bending reflection. Furthermore, the electrode acted as a support for uniformly grown NiFeP nanoarrays to accelerate the charge transport. As extrusion-based 3D printing allows precise control over layer thickness, electrodes of different numbers of layers were prepared. The optimized material consisted of 24 layers of 3DP GC/NiFeP shown OER with an overpotential of 214 mV to reach a current density of 30 mA cm^{-2} in 1.0 M KOH (Figure 6c). As can be seen in Figure 6d, the mass activity of NiFeP on the 3D electrode remains unchanged with the increase in mass loading unlike on carbon paper. Furthermore, water-splitting performance with

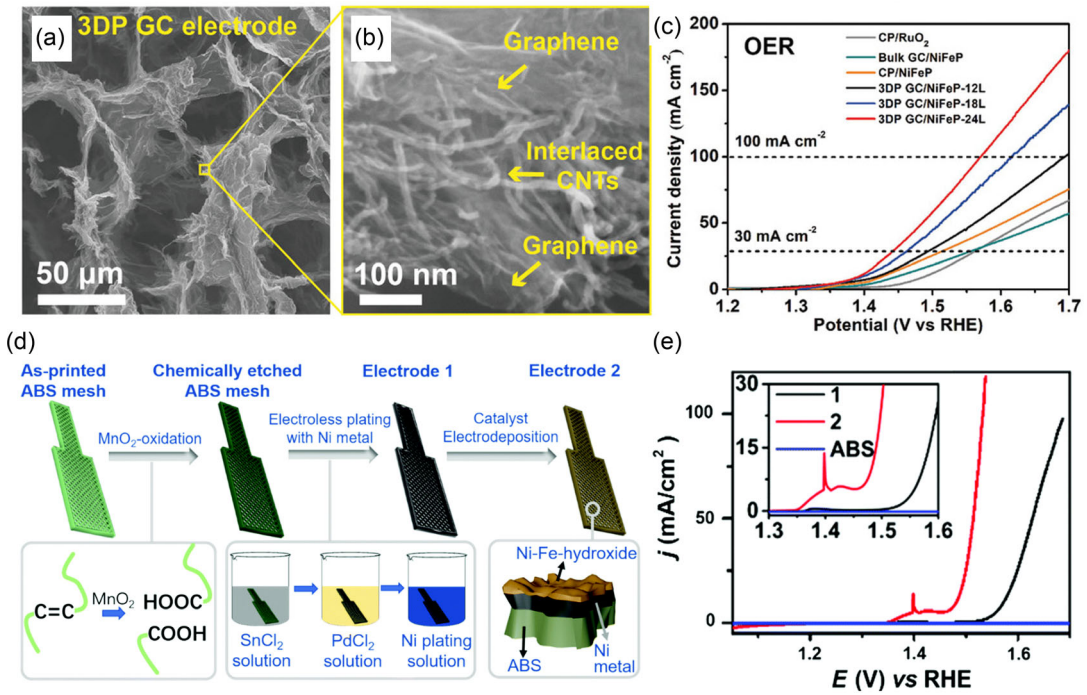

Figure 6. a,b) The SEM images of 3DP-GC electrode. c) Polarization curves for OER. Reproduced with permission.[62] Copyright 2020, Wiley-VCH. d) Schematic illustration of catalyst modification process on ABS mesh electrode. e) The LSV polarization curves. Reproduced with permission.[13] Copyright 2020, The Royal Society of Chemistry.

3DP GC/NiFeP as both cathode and anode was achieved in a voltage of 1.58 V at a current density of 30 mA cm^{-2}. Firstly, integrating 3D printing with phosphidation eliminates the usage of binders, unlike conventional substrates such as metal plates that typically lack adhesion-supporting micro-structured surfaces.[143] Additionally, 3D printing enables the precise fabrication of hierarchical structures that further enhance mass transport and the amount of accessible active sites.[144] However, challenges such as maintaining high conductivity, achieving stronger adhesion without binder, and long-term durability have not been addressed by 3D printing.

4.2.3. Transition Metal Oxides and Hydroxides

Bimetallic iron-nickel (M) oxide/ hydroxide is another emerging category of catalyst due to its OER mechanism involving coordinate formations of MO, MOH, and MOOH.[13,145–147] Moreover, it is pivotal to ensure the electrical and mechanical stability of metals on the electrode surface not to be affected by the harsh environment of electrocatalysis. In a work reported by Liu et al. a polymer-based 3D-printed electrode was made from acrylonitrile-butadiene-styrene (ABS).[13] ABS is a commonly studied polymer for various applications due to its inexpensive nature and low-temperature processability.[148] 3D printing enabled the fabrication of a high surface area ABS polymer mesh. Due to the non-conducting nature of the as-prepared polymer surface, it was functionalized via chemical etching using MnO_2 followed by electroless deposition of nickel. Finally, the Ni–Fe hydroxide catalyst was grown on the functionalized ABS mesh surface. Figure 6d shows a schematic representation of the modification process. The oxidative treatment increased surface area and wrinkling, which the authors claimed is due to selective oxidation of the C═C double bond to carboxylic acid by MnO_2. The modified electrode exhibited excellent OER activity in 1 M KOH with an overpotential of 250 mV at a current density of 10 mA cm^{-2} (Figure 6e). This work thus introduced an excellent alternative for high energy-demanding 3D metal substrate fabrication. Furthermore, the material achieved excellent stability over 10 h. This study presents a low-cost and high surface-area material for catalysis. However, the added modification steps further increase the complexity and time required for catalyst preparation. Also, the reliability of oxidative treatment can potentially limit scalability due to any possible variation.

In 2019, Santos et al. prepared a 3D-printed graphene electrode using commercial conductive graphene/polylactic acid filament and modified the electrode with Ni–Fe(oxy)hydroxide via a chronopotentiometric electrodeposition.[149] The authors studied OER electrocatalytic performance of the material with a varying concentration of Fe. Among these, electrocatalysts with 10% Fe showed onset potential and overpotential values which are only 40 mV and 103 mV higher than state-of-art Ir electrocatalyst. Electrocatalytic activity of 3D electrode/Ni–Fe elevated after 100 and 1000 CV cycles. This has been attributed to the stabilization of reaction intermediates (OH, —O, and —OOH). EIS studies have further substantiated the results and shown that improved performance with 10% Fe is due to adequate exposure of the edge planes and active sites. This study thus reveals that along with exposing adequate surface area, optimization of the composition of active materials can be accomplished to tailor electrocatalytic activity of the material.

In another study, Zhou et al. developed 3D-printed NiFe electrodes as self-support and grew flower-like clusters of $NiFe_2O_4$ nanoneedles covered with FeOOH nanosheets.[150] The 3D hierarchically micro-nano-structured NiFe electrode was prepared via direct writing 3D printing and modified with NiFeOH via a hydrothermal method. The process resulted in numerous interfaces between two metal spheres, benefiting the electron transfer rate and detachment of oxygen bubbles from the electrode surface. Studying OER activity revealed that the material required 220 mV overpotential to obtain 100 mA cm^{-2} and excellent stability over 100 h. This study reveals that, unlike conventional methods of preparing bimetallic foam substrates, 3D printing can override problems such as the nonuniform distribution of active components and the incorporation of external impurities from used precursor materials.

In a work by Kou et al. a 3D-printed Ni (3DPN) electrode modified with carbon-doped NiO has been developed.[151] This electrode was shown to perform alkaline water electrolysis at an exceptionally high current density of 1000 mA cm^{-2} with HER and OER overpotentials of 245 and 425 mV, respectively. This improvement in performance in contrast to the conventional Ni foam (NF)-based electrode, was attributed to the facilitated gas bubble transport through the periodic porous geometry of the electrode. Furthermore, the authors contributed to the development of bifunctional C-$Ni_{1-x}O$/3DPNi for both HER and OER electrodes. The device accomplished an excellent current density of 850 mA cm^{-2} at 2.2 V for at least 16 h.

4.2.4. Hybrid and Composite Materials

In addition to the well-studied materials discussed earlier, there is considerable interest in a diverse array of hybrid and composite materials that offer benefits for water-splitting application.[152–154] Different active materials can be incorporated to prepare electrocatalytic components by synergistically utilizing the combined benefits of each component. An attractive material with great performance in OER is bimetallic carbonate hydroxide. Despite revealing electrocatalytic materials with promising properties, the high mass loading requirement limits their effectiveness.[55] Surface functionalization of the 3D-printed electrodes provides a promising solution to challenges associated with high mass loading.

In this regard, Guo et al. studied the HER activity of free-standing electrodes with the 3D-printed lattice of titanium alloy modified with Co-Ni carbonate hydroxide (CNBH) and copper hydroxide.[155] For this purpose, catalyst support based on titanium alloy, Ti–6Al–4V was prepared via selective laser melting. The lattice was anodized before the electroless deposition of copper, followed by the growing of $Cu(OH)_2$ nanotubes. Finally, Co-Ni carbonate hydroxide was deposited via the hydrothermal method. The as-synthesized material achieved an OER activity at 30 mA cm^{-2} with an overpotential of 355 mV and a Tafel slope of 125.3 mV dec^{-1}. As remarked by the author, the effective 3D design and coating strategies resulted in the formation of hierarchical porous structures resulting in improved electrocatalytic performance. Furthermore, the 3D-printed lattice

exhibited enhanced corrosion resistance and mechanical stability, demonstrating its high suitability for prolonged OER performance in alkaline media. TEM analysis of the modified lattice substantiates the result by revealing that $Cu(OH)_2$ and CNBH are properly anchored with no clear interface. This study was further supported by theoretical evaluation including DFT analysis to explore the synergetic impact of bimetallic compounds on kinetically improved redox processes.

Strategies to facilitate gas transport processes are highly desirable in all gas-evolving reactions including water splitting. Inspired by the hierarchical branches/leaves of a submerged plant, Chen et al. demonstrated a preparation strategy for a five-layered electrocatalyst system, using a 3D-printed supporting electrode.[156] The material fabrication was done as follows: firstly, a printable ink was prepared using cellulose nanofiber, bacterial cellulose, and dicyanamide, which was 3D-printed via an extrusion method; secondly, the prepared 3D electrode was immersed in an $Fe(NO_3)^3$ solution—followed by freeze-drying and carbonization via melamine vapour. Finally, the resulting material was electrodeposited with nickel to obtain the desired product designated as 3DC-Fe-CNTs-Ni/$Ni(OH)^2$. This material accomplished multifunctionality in water splitting and battery applications benefitting from the combined effect of different active materials. Wherein, single-Fe-atom doping of $Ni/Ni(OH)^2$ enabled improved water-splitting performance. This was attributed to the incorporation of Fe source into the 3D framework with improved exposed active sites. The material was analyzed for its HER and OER activities, along with other electrochemical applications. The electrode delivered a current density of $30\,mA\,cm^{-2}$, at overpotentials of 175 and 108 mV for OER and HER respectively. Moreover, the overall water-splitting cell achieved reasonable stability with a low voltage of 1.51 V to obtain a current density of $30\,mA\,cm^{-2}$ for 10 h.

5. Perspective and Conclusion

Recently 3D-printing technologies have found application in electrocatalytic applications. Freedom of design and rapid prototyping ability of these techniques have been utilized to convert computer-aided designed structures to functional materials with tailored properties. Additionally, 3D printing can create complex geometries with virtually no limit—to enhance the stability and activity of the electrocatalytic materials. Among the numerous options available, four main 3D-printing techniques have been implemented for electrocatalytic applications; FMA for its cost-effectiveness and simplicity, DIW as a high-resolution and easy processible method, SLM for high accuracy and material selection—and SLA is identified as the high-resolution and reasonably fast technique. Despite exploring numerous promising first-generation prototypes, these technologies are still under research and development due to slow production speed, material inconsistencies, etc. Based on the current scenario, 3D printing cannot completely replace conventional fabrication methods but rather complement them.

On the contrary, electrocatalytic water splitting is at the forefront as a technology for solving the global energy crisis and environmental depletion by producing green hydrogen. However, repositioning this technology from academics to industry remains an unresolved task. The barriers include costs associated with components for electrochemical, mechanical, and structural integration. In the search for alternative electrocatalysts, transition metals, their compounds, alloys, and composite with other materials as well as 2D materials with structural tunability have been explored. There are two main strategies to enhance their electrocatalytic performance: increasing the active surface area via support-based manufacturing and increasing the intrinsic activity via structural engineering. In practice, long-term stability and sustained activity are generally best achieved by balancing both approaches. In this review, we discussed the application of 3D printing combined with surface modification using emerging non-noble metal active materials to fabricate electrode-electrocatalyst system for HER and OER reactions. Based on our analysis, we have made the following conclusions and perspectives.

First, the industrialization of bespoke device developments is far from realization. This is primarily attributed to current density and durability, which are inadequate to compete with state-of-the-art electrocatalysts. Upscaling current density while maintaining electrochemical conversion efficiency is still an open question. This is raised by problems such as inconsistent catalyst coverage, poor adhesion and long-term durability. Another practical challenge for 3D-printed electrocatalytic applications is material compatibility. Production of conductive 3D materials such as pure metal and stainless steel requires energy-demanding processes, such as selective laser melting and sintering and offers sub-optimal resolution. Furthermore, activation and pre-functionalization processes are necessary before modifying the surface with electroactive materials due to the poor conductivity of other materials including polymer and carbon. Despite the enormous development of 3D printing, further exploration and creativity are necessary to establish a level of excellence similar to noble metals. Integrating advanced fabrication techniques such as ALD, electrodeposition, dip-coating, and spray-coating provides promising pathways for developing high-performance materials and electrodes. These methods offer opportunities for precise control over uniform deposition, material properties, and tailored geometries that improve functionality. However, these techniques encounter several common challenges, including problems with adhesion, uniformity, and optimization of processing parameters for complex geometries, whereas 3D printing offers limitless design possibilities.

As already discussed, OER impedes the overall kinetics of the water-splitting reaction due to the complex reaction mechanism and formation of multiple intermediates. Therefore, experimental calculations are insufficient to fully comprehend the reaction mechanism. Most studies discussed did not include theoretical approaches, which is crucial to understanding the interaction between integrated electrodes and catalysts. Theoretical approaches such as ab initio density functional theory (DFT) alleviate these challenges. In light of these understandings, no ideal devices for water splitting have been reported yet.

Despite these challenges, the potential of surface functionalization of 3D-printed material to broaden the horizon of electrocatalytic water-splitting applications is still within reach. According to our perspective, the literature discussed earlier explores other electrochemically active 2D materials such as metal–organic frameworks (MOFs), germanene, hematite, geothite, phosphorene, and borophene. Carbonaceous materials

have been known for replacing noble-metal-based electrodes. 3D printing of carbon materials has been realized via techniques such as FDM and extrusion-based 3D printing. However, these techniques offer limited design freedom and poor surface finishing. Alternatively, integrating polymer 3D printing and consequent pyrolysis creates a new avenue for fabricating 3D carbon materials with precise control over geometry and properties.[157] This approach offers significant advantages over conventional electrode fabrication methods, allowing for customizable, scalable designs at potentially lower costs. SLA and direct laser writing using two-photon polymerization (DLW-2PP) are the two foremost 3D-printing techniques that excel in this domain.[60,158,159] These approaches surpass the limitations of conventional 3D printing by achieving resolutions in the micron to sub-micron range. SLA has already been established as a high-precision 3D-printing technique for complex polymer geometries. Materials with tailored properties can be generated by utilizing 3D polymer fabricated via SLA and transforming it into carbon structures through pyrolysis. In addition to SLA, DLW-2PP introduces a significant advancement in this field. Usually, the 2PP process is triggered when an initiator molecule in a photosensitive resin absorbs a pair of near-infrared (NIR) photons. This approach further surpasses the limitations of conventional 3D printing by achieving resolutions below the diffraction limit, which enables mask-less creation of polymer structures with lateral line widths that are less than 100 nm.[160] This precise control over surface features is vital for optimizing electrocatalytic activity, where surface area and conductivity directly impact efficiency, making it highly beneficial for electrocatalysis. This technique has found extensive application in various fields such as 2D/3D photonic crystals,[161–167] 3D magnetic structures,[168,169] nano-tools,[170] and micro-rotors.[171] These finely detailed polymer structures when pyrolysed, convert into carbon-based materials while preserving their intricate features. From our perspective, DLW-2PP with pyrolysis holds great promise for electrocatalytic water-splitting applications. Moreover, conductive polymers are another class of emerging materials which have not yet been explored for 3D-printed water-splitting electrodes. Incorporating conductive polymers could enhance the mechanical stability and electrical conductivity of 3D-printed structures, addressing current limitations. Even though theoretical approaches are time-consuming and intricate, they can bring about progress in water electrolyser research in a prompt manner. Besides, by seizing the opportunities of machine learning and artificial intelligence, researchers can unravel the complexities of 3D electrocatalyst design to accelerate sustainable hydrogen production strategies. We thereby conclude that surface functionalization of the 3D printed electrode can greatly contribute to the advancement of the global water electrolyser industry, as well as other electrochemical applications—including battery and fuel cells. Therefore, added concerns must be promoted to overcome existing energy challenges and to fabricate ground-breaking devices.

Acknowledgements

This work was supported by the Energy Futures Seed Fund and Research Development Fund (RDF) Studentship Scheme at Northumbria University and the Engineering and Physical Sciences Research Council (EPSRC) grants EP/N00762X/1, EP/V040030/1, EP/Y016440/1, and EP/Y003551/1.

Conflict of Interest

The authors declare no conflict of interest.

Keywords

2D materials, 3D-printing technology, 3D-printed electrodes, electrocatalytic water splitting, surface functionalized 3D electrodes

Received: August 20, 2024
Revised: November 7, 2024
Published online: January 16, 2025

[1] S. A. Neto, T. F. Moreira, P. Olivi, *Int. J. Hydrogen Energy* **2019**, *44*, 16.
[2] L. Schlapbach, A. Züttel, *Nature* **2001**, *414*, 353.
[3] H. Ozcan, R. S. El-Emam, S. Celik, B. Amini Horri, *Clean. Chem. Eng.* **2023**, *8*, 100115.
[4] Z. Y. Yu, Y. Duan, X. Y. Feng, X. Yu, M. R. Gao, S. H. Yu, *Adv. Mater.* **2021**, *33*, 31.
[5] J. Hou, Y. Wu, B. Zhang, S. Cao, Z. Li, L. Sun, *Adv. Funct. Mater.* **2019**, *29*, 20.
[6] L. Zhang, G. Li, H. Yan, S. Chen, H. Tu, J. Su, M. Qiu, S. Zhao, T. Sun, Q. Li, L. Ding, Y. Wang, *Composite Part B* **2022**, *245*, 110189.
[7] C. Y. Lee, A. C. Taylor, S. Beirne, G. G. Wallace, *Adv. Mater. Technol.* **2019**, *4*, 10.
[8] A. Ursua, L. M. Gandia, P. Sanchis, *Proc. IEEE* **2012**, *100*, 2.
[9] K. Shah, R. Dai, M. Mateen, Z. Hassan, Z. Zhuang, C. Liu, M. Israr, W. C. Cheong, B. Hu, R. Tu, C. Zhang, X. Chen, Q. Peng, C. Chen, Y. Li, *Angew. Chem. Int. Ed.* **2022**, *61*, 4.
[10] A. Raveendran, M. Chandran, R. Dhanusuraman, *RSC Adv.* **2023**, *13*, 6.
[11] N. Cheng, S. Stambula, D. Wang, M. N. Banis, J. Liu, A. Riese, B. Xiao, R. Li, T. K. Sham, L. M. Liu, G. A. Botton, X. Sun, *Nat. Commun.* **2016**, *7*, 13638.
[12] M. A. Abbas, J. H. Bang, *Chem. Mater.* **2015**, *27*, 21.
[13] S. Liu, R. Liu, D. Gao, I. Trentin, C. Streb, *Chem. Commun.* **2020**, *56*, 60.
[14] Q. Feng, Q. Wang, Z. Zhang, Y. Xiong, H. Li, Y. Yao, X. Z. Yuan, M. C. Williams, M. Gu, H. Chen, H. Li, H. Wang, *Appl. Catal. B: Environ.* **2019**, *244*, 494.
[15] Y. Shi, Z. R. Ma, Y. Y. Xiao, Y. C. Yin, W. M. Huang, Z. C. Huang, Y. Z. Zheng, F. Y. Mu, R. Huang, G. Y. Shi, Y. Y. Sun, X. H. Xia, W. Chen, *Nat. Commun.* **2021**, *12*, 1.
[16] M. Ledendecker, S. Geiger, K. Hengge, J. Lim, S. Cherevko, A. M. Mingers, D. Göhl, G. V. Fortunato, D. Jalalpoor, F. Schüth, C. Scheu, K. J. Mayrhofer, *Nano Res.* **2019**, *12*, 9.
[17] L. Cao, Q. Luo, J. Chen, L. Wang, Y. Lin, H. Wang, X. Liu, X. Shen, W. Zhang, W. Liu, Z. Qi, Z. Jiang, J. Yang, T. Yao, *Nat. Commun.* **2019**, *10*, 1.
[18] J. Yu, Q. He, G. Yang, W. Zhou, Z. Shao, M. Ni, *ACS Catal.* **2019**, *9*, 11.
[19] J. Yu, G. Li, H. Liu, L. Zhao, A. Wang, Z. Liu, H. Li, H. Liu, Y. Hu, W. Zhou, *Adv. Funct. Mater.* **2019**, *29*, 22.
[20] Y. Zheng, Y. Jiao, Y. Zhu, L. H. Li, Y. Han, Y. Chen, M. Jaroniec, S. Z. Qiao, *J. Am. Chem. Soc.* **2016**, *138*, 49.
[21] Y. Zhang, T. Liu, D. Dong, X. Jiang, C. Deng, M. Liu, *Int. J. Hydrogen Energy* **2020**, *45*, 46.

[22] L. Zhang, Q. Fan, K. Li, S. Zhang, X. Ma, *Sustainable Energy Fuels* **2020**, *4*, 11.
[23] Q. Wang, D. Ohare, *Chem. Rev.* **2012**, *112*, 7.
[24] D. Voiry, M. Salehi, R. Silva, T. Fujita, M. Chen, T. Asefa, V. B. Shenoy, G. Eda, M. Chhowalla, *Nano Lett.* **2013**, *13*, 12.
[25] V. Vij, S. Sultan, A. M. Harzandi, A. Meena, J. N. Tiwari, W. G. Lee, T. Yoon, K. S. Kim, *ACS Catal.* **2017**, *7*, 10.
[26] M. Gong, D. Y. Wang, C. C. Chen, B. J. Hwang, H. Dai, *Nano Res.* **2016**, *9*, 1.
[27] Y. Luo, Z. Zhang, F. Yang, J. Li, Z. Liu, W. Ren, S. Zhang, B. Liu, *Energy Environ. Sci.* **2021**, *14*, 8.
[28] V. Tripathi, S. Jain, D. Kabra, L. S. Panchakarla, A. Dutta, *Nanoscale Adv.* **2022**, *5*, 237.
[29] J. Li, Y. Wang, T. Zhou, H. Zhang, X. Sun, J. Tang, L. Zhang, A. M. Al-Enizi, Z. Yang, G. Zheng, *J. Am. Chem. Soc.* **2015**, *137*, 45.
[30] J. N. Hansen, H. Prats, K. K. Toudahl, N. Mørch Secher, K. Chan, J. Kibsgaard, I. Chorkendorff, *ACS Energy Lett.* **2021**, *6*, 4.
[31] P. Hota, A. Das, D. K. Maiti, *Int. J. Hydrogen Energy* **2023**, *48*, 2.
[32] L. Tian, Z. Li, M. Song, J. Li, *Nanoscale* **2021**, *13*, 28.
[33] T. Liu, P. Li, N. Yao, G. Cheng, S. Chen, W. Luo, Y. Yin, *Angew. Chem. Int. Ed.* **2019**, *58*, 14.
[34] S. Bai, M. Yang, J. Jiang, X. He, J. Zou, Z. Xiong, G. Liao, S. Liu, *NPJ 2D Mater. Appl.* **2021**, *5*, 1.
[35] X. Bai, C. Ling, L. Shi, Y. Ouyang, Q. Li, J. Wang, *Sci. Bull.* **2018**, *63*, 21.
[36] W. Chen, W. Wei, K. Wang, J. Cui, X. Zhu, K. Ostrikov, *Nanoscale* **2021**, *13*, 34.
[37] C. Chen, Z. Fu, F. Qi, Y. Chen, G. Meng, Z. Chang, F. Kong, L. Zhu, H. Tian, H. Huang, X. Cui, J. Shi, *Angew. Chem. Int. Ed.* **2022**, *61*, 32.
[38] L. Zhu, J. Huang, G. Meng, T. Wu, C. Chen, H. Tian, Y. Chen, F. Kong, Z. Chang, X. Cui, J. Shi, *Nat. Commun.* **2023**, *14*, 1.
[39] Q. Li, C. Chen, W. Luo, X. Yu, Z. Chang, F. Kong, L. Zhu, Y. Huang, H. Tian, X. Cui, J. Shi, *Adv. Energy Mater.* **2024**, *14*, 17.
[40] Y. Ying, M. P. Browne, M. Pumera, *Sustainable Energy Fuels* **2020**, *4*, 7.
[41] T. Chu, S. Park, K. Fu, *Carbon Energy* **2021**, *3*, 3.
[42] M. P. Browne, E. Redondo, M. Pumera, *Chem. Rev.* **2020**, *120*, 5.
[43] C. W. Foster, M. P. Down, Y. Zhang, X. Ji, S. J. Rowley-Neale, G. C. Smith, P. J. Kelly, C. E. Banks, *Sci. Rep.* **2017**, *7*, 42233.
[44] R. J. Morrison, K. N. Kashlan, C. L. Flanangan, J. K. Wright, G. E. Green, S. J. Hollister, K. J. Weatherwax, *Clin. Transl. Sci.* **2015**, *8*, 5.
[45] M. R. Khosravani, T. Reinicke, *Sens. Actuators A: Phys.* **2020**, *305*, 111916.
[46] M. P. Browne, J. Plutnar, A. M. Pourrahimi, Z. Sofer, M. Pumera, *Adv. Energy Mater.* **2019**, *9*, 26.
[47] E. MacDonald, R. Wicker, *Science* **2016**, *353*, 6307.
[48] M. Gebler, A. J. Schoot Uiterkamp, C. Visser, *Energy Policy* **2014**, *74*, 158.
[49] X. Su, X. Li, C. Y. A. Ong, T. S. Herng, Y. Wang, E. Peng, J. Ding, *Adv. Sci.* **2019**, *6*, 6.
[50] M. Sánchez-Molina, E. Amores, N. Rojas, M. Kunowsky, *Int. J. Hydrogen Energy* **2021**, *46*, 79.
[51] G. Chisholm, P. J. Kitson, N. D. Kirkaldy, L. G. Bloor, L. Cronin, *Energy Environ. Sci.* **2014**, *7*, 9.
[52] C. Y. Lee, A. C. Taylor, A. Nattestad, S. Beirne, G. G. Wallace, *Joule* **2019**, *3*, 8.
[53] N. Lindner, A. Blaeser, *Front. Bioeng. Biotechnol.* **2022**, *10*, 855042.
[54] B. Hüner, N. Demir, M. F. Kaya, *Fuel* **2023**, *331*, 125971.
[55] S. Chang, X. Huang, C. Y. Aaron Ong, L. Zhao, L. Li, X. Wang, J. Ding, *J. Mater. Chem. A* **2019**, *7*, 31.
[56] A. Hofer, S. Wachter, D. Döhler, A. Laube, B. Sánchez Batalla, Z. Fu, C. Weidlich, T. Struckmann, C. Körner, J. Bachmann, *Electrochim. Acta* **2022**, *417*, 140308.
[57] Q. Wen, Y. Zhao, Y. Liu, H. Li, T. Zhai, *Small* **2022**, *18*, 4.
[58] M. I. Jamesh, Y. Kuang, X. Sun, *ChemCatChem* **2019**, *11*, 6.
[59] L. C. Seitz, C. F. Dickens, K. Nishio, Y. Hikita, J. Montoya, A. Doyle, C. Kirk, A. Vojvodic, H. Y. Hwang, J. K. Norskov, T. F. Jaramillo, *Science* **2016**, *353*, 6303.
[60] B. Rezaei, J. Y. Pan, C. Gundlach, S. S. Keller, *Mater. Des.* **2020**, *193*, 108834.
[61] A. Ambrosi, M. Pumera, *Adv. Funct. Mater.* **2018**, *28*, 27.
[62] M. Peng, D. Shi, Y. Sun, J. Cheng, B. Zhao, Y. Xie, J. Zhang, W. Guo, Z. Jia, Z. Liang, L. Jiang, *Adv. Mater.* **2020**, *32*, 23.
[63] R. Gusmão, M. P. Browne, Z. Sofer, M. Pumera, *Electrochem. Commun.* **2019**, *102*, 83.
[64] B. Yu, B. Chan Choi, Y. Myung, J. Rae Kim, H. Chan Kim, Y. W. Choi, *Appl. Surf. Sci.* **2023**, *614*, 155741.
[65] F. Novotný, V. Urbanová, J. Plutnar, M. Pumera, *ACS Appl. Mater. Interfaces* **2019**, *11*, 38.
[66] M. P. Browne, F. Novotný, Z. Sofer, M. Pumera, *ACS Appl. Mater. Interfaces* **2018**, *10*, 46.
[67] J. Zhang, C. M. Li, *Chem. Soc. Rev.* **2012**, *41*, 21.
[68] L. W. Tang, Y. Alias, P. K. Jiwanti, P. M. Woi, *Trends Environ. Anal. Chem.* **2024**, *41*, e00225.
[69] A. Urtiaga, *Curr. Opin. Electrochem.* **2021**, *27*, 100691.
[70] D. P. Rocha, R. G. Rocha, S. V. Castro, M. A. Trindade, R. A. Munoz, E. M. Richter, L. Angnes, *Electrochem. Sci. Adv.* **2022**, *2*, 5.
[71] S. Srinivasan, J. Santo, P. K. Penumakala, *J. Energy Storage* **2022**, *56*, 106043.
[72] P. Jiang, Z. Ji, X. Wang, F. Zhou, *J. Mater. Chem. C* **2020**, *8*, 36.
[73] V. Urbanová, J. Plutnar, M. Pumera, *Appl. Mater. Today* **2021**, *24*, 101131.
[74] R. Gusmão, Z. Sofer, P. Marvan, M. Pumera, *Nanoscale* **2019**, *11*, 20.
[75] Y. Xun, K. Zhang, W. Jonhson, J. Ding, *APL Mater.* **2023**, *11*, 6.
[76] S. Mojabi, N. Afsahi, N. Naseri, *Int. J. Hydrogen Energy* **2024**, *49*, 116.
[77] M. S. Alnarabiji, S. C. E. Tsang, A. H. Mahadi, *Fuel* **2024**, *357*, 129741.
[78] A. Ambrosi, R. R. S. Shi, R. D. Webster, *J. Mater. Chem. A* **2020**, *8*, 42.
[79] J. Chen, P. Wu, F. Bu, Y. Gao, X. Liu, C. Guan, *DeCarbon* **2023**, *2*, 100019.
[80] X. Sheng, A. Wang, Z. Wang, H. Liu, J. Wang, C. Li, *Front. Bioeng. Biotechnol.* **2022**, *10*, 850110.
[81] M. Deka, N. Sinha, R. Das, N. K. Hazarika, H. Das, B. Daurai, M. Gogoi, *Anal. Methods* **2023**, *16*, 4.
[82] S. Bose, S. F. Robertson, A. Bandyopadhyay, *Acta Biomater.* **2018**, *66*, 6.
[83] N. H. Mohd Yusoff, C. H. Chong, Y. K. Wan, K. H. Cheah, V. L. Wong, *J. Water Process Eng.* **2023**, *51*, 103410.
[84] J. Wang, X. Yue, Y. Yang, S. Sirisomboonchai, P. Wang, X. Ma, A. Abudula, G. Guan, *J. Alloys Compd.* **2020**, *819*, 153346.
[85] T. Kim, Y. Song, J. Kang, S. K. Kim, S. Kim, *Int. J. Hydrogen Energy* **2022**, *47*, 59.
[86] Y. Gong, J. Yao, P. Wang, Z. Li, H. Zhou, C. Xu, *Chin. J. Chem. Eng.* **2022**, *43*, 282.
[87] J. Li, L. Li, J. Wang, A. Cabot, Y. Zhu, *ACS Energy Lett.* **2024**, *9*, 3.
[88] S. Gupta, M. K. Patel, A. Miotello, N. Patel, *Adv. Funct. Mater.* **2020**, *30*, 1.
[89] B. You, Y. Sun, *Acc. Chem. Res.* **2018**, *51*, 7.
[90] E. Fabbri, T. J. Schmidt, *ACS Catal.* **2018**, *8*, 10.
[91] S. Wang, A. Lu, C. J. Zhong, *Nano Converg.* **2021**, *8*, 1.
[92] J. Zhu, L. Hu, P. Zhao, L. Y. S. Lee, K. Y. Wong, *Chem. Rev.* **2020**, *120*, 2.
[93] E. A. Paoli, F. Masini, R. Frydendal, D. Deiana, C. Schlaup, M. Malizia, T. W. Hansen, S. Horch, I. E. Stephens, I. Chorkendorff, *Chem. Sci.* **2015**, *6*, 1.

[94] J. R. C. Dizon, A. H. Espera, Q. Chen, R. C. Advincula, *Addit. Manuf.* **2018**, *20*, 44.
[95] C. K. Su, *Anal. Chim. Acta* **2021**, *1158*, 338348.
[96] A. Ambrosi, M. Pumera, *Chem. Soc. Rev.* **2016**, *45*, 10.
[97] K. Rajan, M. Samykano, K. Kadirgama, W. S. W. Harun, M. M. Rahman, *Int. J. Adv. Manuf. Technol.* **2022**, *120*, 3.
[98] R. F. Quero, G. Domingos Da Silveira, J. A. Fracassi Da Silva, D. P. D. Jesus, *Lab Chip* **2021**, *21*, 19.
[99] C. Zhu, T. Y. J. Han, E. B. Duoss, A. M. Golobic, J. D. Kuntz, C. M. Spadaccini, M. A. Worsley, *Nat. Commun.* **2015**, *6*, 6962.
[100] J. A. Lewis, *Adv. Funct. Mater.* **2006**, *16*, 17.
[101] S. Waheed, J. M. Cabot, N. P. Macdonald, T. Lewis, R. M. Guijt, B. Paull, M. C. Breadmore, *Lab Chip* **2016**, *16*, 11.
[102] B. C. Gross, J. L. Erkal, S. Y. Lockwood, C. Chen, D. M. Spence, *Anal. Chem.* **2014**, *86*, 7.
[103] F. P. Melchels, J. Feijen, D. W. Grijpma, *Biomaterials* **2010**, *31*, 24.
[104] L. S. S. Magalhães, F. E. P. Santos, C. de Maria Vaz Elias, S. Afewerki, G. F. Sousa, A. S. Furtado, F. R. Marciano, A. O. Lobo, *J. Funct. Biomater.* **2020**, *11*, 1.
[105] C. Y. Lee, A. C. Taylor, S. Beirne, G. G. Wallace, *Adv. Energy Mater.* **2017**, *7*, 21.
[106] Q. Cao, Y. Bai, J. Zhang, Z. Shi, J. Y. H. Fuh, H. Wang, *Mater. Des.* **2020**, *191*, 108691.
[107] Y. J. Kim, A. Lim, J. M. Kim, D. Lim, K. H. Chae, E. N. Cho, H. J. Han, K. U. Jeon, M. Kim, G. H. Lee, G. R. Lee, H. S. Ahn, H. S. Park, H. Kim, J. Y. Kim, Y. S. Jung, *Nat. Commun.* **2020**, *11*, 1.
[108] Q. Wu, T. Yao, M. Sheng, J. Shi, F. Lv, *Mater. Res. Express.* **2019**, *6*, 11.
[109] J. Wang, Y. Gao, H. Kong, J. Kim, S. Choi, F. Ciucci, Y. Hao, S. Yang, Z. Shao, J. Lim, *Chem. Soc. Rev.* **2020**, *49*, 24.
[110] C. Panda, P. W. Menezes, M. Zheng, S. Orthmann, M. Driess, *ACS Energy Lett.* **2019**, *4*, 3.
[111] S. Li, M. Li, Y. Ni, *Appl. Catal. B: Environ.* **2020**, *268*, 118392.
[112] M. Łuba, T. Mikołajczyk, M. Kuczyński, B. Pierożyński, I. M. Kowalski, *Catalysts* **2021**, *11*, 4.
[113] F. Rocha, R. Delmelle, C. Georgiadis, J. Proost, *J. Environ. Chem. Eng.* **2022**, *10*, 3.
[114] R. A. Márquez, K. Kawashima, Y. J. Son, R. Rose, L. A. Smith, N. Miller, O. A. Carrasco Jaim, H. Celio, C. B. Mullins, *ACS Appl. Mater. Interfaces* **2022**, *14*, 37.
[115] R. J. Toh, Z. Sofer, J. Luxa, D. Sedmidubský, M. Pumera, *Chem. Commun.* **2017**, *53*, 21.
[116] S. Bertolazzi, J. Brivio, A. Kis, *ACS Nano* **2011**, *5*, 12.
[117] R. Ganatra, Q. Zhang, *ACS Nano* **2014**, *8*, 5.
[118] R. W. Johnson, A. Hultqvist, S. F. Bent, *Mater. Today* **2014**, *17*, 5.
[119] S. E. Koponen, P. G. Gordon, S. T. Barry, *Polyhedron* **2016**, *108*, 59.
[120] P. Sahatiya, S. Kannan, S. Badhulika, *Appl. Mater. Today* **2018**, *13*, 91.
[121] J. E. Huddy, W. J. Scheideler, *STAR Protoc.* **2022**, *3*, 3.
[122] C. Iffelsberger, S. Ng, M. Pumera, *Appl. Mater. Today* **2020**, *20*, 100654.
[123] E. Vaněčková, M. Bouša, R. Sokolová, P. Moreno-García, P. Broekmann, V. Shestivska, J. Rathouský, M. Gál, T. Sebechlebská, V. Kolivoška, *J. Electroanal. Chem.* **2020**, *858*, 113763.
[124] Y. Gogotsi, B. Anasori, *ACS Nano* **2019**, *13*, 8.
[125] X. Jiang, A. V. Kuklin, A. Baev, Y. Ge, H. Ågren, H. Zhang, P. N. Prasad, *Phys. Rep.* **2020**, *848*, 1.
[126] M. Naguib, M. Kurtoglu, V. Presser, J. Lu, J. Niu, M. Heon, L. Hultman, Y. Gogotsi, M. W. Barsoum, *Adv. Mater.* **2011**, *23*, 37.
[127] Q. Tang, Z. Zhou, *Prog. Mater. Sci.* **2013**, *58*, 8.
[128] X. Li, C. Wang, Y. Cao, G. Wang, *Chem. Asian J.* **2018**, *13*, 19.
[129] B. Anasori, M. R. Lukatskaya, Y. Gogotsi, *Nat. Rev. Mater.* **2017**, *2*, 2.
[130] Z. W. Seh, K. D. Fredrickson, B. Anasori, J. Kibsgaard, A. L. Strickler, M. R. Lukatskaya, Y. Gogotsi, T. F. Jaramillo, A. Vojvodic, *ACS Energy Lett.* **2016**, *1*, 3.
[131] B. Ding, W. J. Ong, J. Jiang, X. Chen, N. Li, *Appl. Surf. Sci.* **2020**, *500*, 143987.
[132] W. Yang, S. Chen, *Chem. Eng. J.* **2020**, *393*, 124726.
[133] K. P. Akshay Kumar, K. Ghosh, O. Alduhaish, M. Pumera, *Electrochem. Commun.* **2021**, *122*, 106890.
[134] Z. Ge, Z. He, *RSC Adv.* **2015**, *5*, 46.
[135] Y. Zhang, J. Gao, D. Peng, M. Guangyao, X. Liu, *Ceram. Int.* **2004**, *30*, 6.
[136] L. Chen, S. Zhou, M. Li, F. Mo, S. Yu, J. Wei, *Catalysts* **2022**, *12*, 10.
[137] B. Hüner, N. Demir, M. F. Kaya, *ACS Omega* **2023**, *8*, 6.
[138] B. Hüner, N. Demir, M. F. Kaya, *Int. J. Hydrogen Energy* **2022**, *47*, 24.
[139] I. J. Brown, S. Sotiropoulos, *J. Appl. Electrochem.* **2001**, *31*, 11.
[140] K. M. Cole, S. Prabhudev, G. A. Botton, D. W. Kirk, S. J. Thorpe, *ACS Appl. Nano Mater.* **2020**, *3*, 10.
[141] P. J. Kitson, R. J. Marshall, D. Long, R. S. Forgan, L. Cronin, *Angew. Chem.* **2014**, *126*, 47.
[142] C. Hu, C. Lv, S. Liu, Y. Shi, J. Song, Z. Zhang, J. Cai, A. Watanabe, *Catalysts* **2020**, *10*, 2.
[143] Q. Kang, M. Li, J. Shi, Q. Lu, F. Gao, *ACS Appl. Mater. Interfaces* **2020**, *12*, 17.
[144] Y. Yang, R. Su, D. Wang, H. Zhang, C. Shang, S. Wang, H. Li, *Renewables* **2024**, *2*, 4.
[145] C. Liang, P. Zou, A. Nairan, Y. Zhang, J. Liu, K. Liu, S. Hu, F. Kang, H. J. Fan, C. Yang, *Energy Environ. Sci.* **2020**, *13*, 1.
[146] L. Trotochaud, S. L. Young, J. K. Ranney, S. W. Boettcher, *J. Am. Chem. Soc.* **2014**, *136*, 18.
[147] X. Xu, C. Li, J. G. Lim, Y. Wang, A. Ong, X. Li, E. Peng, J. Ding, *ACS Appl. Mater. Interfaces* **2018**, *10*, 36.
[148] K. R. Hart, E. D. Wetzel, *Eng. Fracture Mech.* **2017**, *177*, 1.
[149] P. L. dos Santos, S. J. Rowley-Neale, A. G. Ferrari, J. A. Bonacin, C. E. Banks, *ChemElectroChem* **2019**, *6*, 22.
[150] B. Zhou, Y. Tang, Z. Jiao, P. Wan, Q. Hu, X. J. Yang, *ACS Appl. Nano Mater.* **2023**, *6*, 6.
[151] T. Kou, S. Wang, T. Zhang, R. Wu, W. Chen, S. Baker, E. Duoss, C. Spadaccini, C. Zhu, Y. Li, *Adv. Energy Mater.* **2020**, *10*, 46.
[152] M. Moazzam Khan, S. Imran Abbas Shah, M. Ammar Hassan Shah, M. Najam-ul Haq, N. H. Alotaibi, S. Mohammad, I. Zada, M. Naeem Ashiq, S. I. Allakhverdiev, *J. Electroanal. Chem.* **2024**, *967*, 118450.
[153] H. Pang, T. Gao, W. Zhao, L. Liu, E. Liu, H. Wen, T. Sun, *Fuel* **2024**, *374*, 132532.
[154] S. Y. Bae, I. Y. Jeon, J. Mahmood, J. B. Baek, *Chem. Eur. J.* **2018**, *24*, 69.
[155] B. Guo, J. Kang, T. Zeng, H. Qu, S. Yu, H. Deng, J. Bai, *Adv. Sci.* **2022**, *9*, 24.
[156] Y. Chen, Y. Cai, R. Yu, X. Pan, J. Zhang, Z. Wang, X. Xiao, J. Wu, L. Xu, L. Mai, *Chem. Eng. J.* **2022**, *446*, 136804.
[157] Y. M. Eggeler, K. C. Chan, Q. Sun, A. D. Lantada, D. Mager, R. Schwaiger, P. Gumbsch, R. Schröder, W. Wenzel, J. G. Korvink, M. Islam, *Adv. Funct. Mater.* **2024**, *34*, 20.
[158] S. Maruo, O. Nakamura, S. Kawata, *Opt. Lett.* **1997**, *22*, 2.
[159] P. Serles, M. Haché, J. Tam, A. Maguire, T. Li, G. Wang, K. Sebastian, J. Lou, C. Jia, P. M. Ajayan, J. Howe, Y. Zou, T. Filleter, *Carbon* **2023**, *201*, 161.
[160] J. Fischer, M. Wegener, *Laser Photonics Rev.* **2013**, *7*, 1.
[161] M. P. Taverne, X. Zheng, Y. S. J. Chen, K. A. Morgan, L. Chen, N. M. Palakkool, D. Rezaie, H. Awachi, J. G. Rarity, D. W. Hewak, H. Chung-Che, Y. L. D. Ho, *ACS Appl. Opt. Mater.* **2023**, *1*, 5.

[162] L. Chen, K. A. Morgan, G. A. Alzaidy, C. C. Huang, Y. L. D. Ho, M. P. Taverne, X. Zheng, Z. Ren, Z. Feng, I. Zeimpekis, D. W. Hewak, J. G. Rarity, *ACS Photonics* **2019**, *6*, 5.
[163] F. Ortiz-Huerta, L. Chen, M. Taverne, J. P. Hadden, M. Johnson, Y. L. D. Ho, J. G. Rarity, *Opt. Express* **2018**, *26*, 25.
[164] J. D. Lin, Y. L. Daniel Ho, L. Chen, M. Lopez-Garcia, S. A. Jiang, M. P. Taverne, C. R. Lee, J. G. Rarity, *ACS Omega* **2018**, *3*, 11.
[165] L. Chen, M. Lopez-Garcia, M. P. C. Taverne, X. Zheng, Y.-L. D. Ho, J. Rarity, *Opt. Lett.* **2017**, *42*, 8.
[166] Y. Hu, B. T. Miles, Y. L. D. Ho, M. P. Taverne, L. Chen, H. Gersen, J. G. Rarity, C. F. Faul, *Adv. Opt. Mater.* **2017**, *5*, 3.
[167] L. Chen, M. P. C. Taverne, X. Zheng, J.-D. Lin, R. Oulton, M. Lopez-Garcia, Y.-L. D. Ho, J. G. Rarity, *Opt. Express* **2015**, *23*, 20.
[168] M. Hunt, M. Taverne, J. Askey, A. May, A. Van Den Berg, Y. L. D. Ho, J. Rarity, S. Ladak, *Materials* **2020**, *13*, 3.
[169] V. Harinarayana, Y. C. Shin, *Opt. Laser Technol.* **2021**, *142*, 107180.
[170] D. B. Phillips, M. J. Padgett, S. Hanna, Y. L. Ho, D. M. Carberry, M. J. Miles, S. H. Simpson, *Nat. Photonics* **2014**, *8*, 5.
[171] U. G. Būtaitė, G. M. Gibson, Y. L. D. Ho, M. Taverne, J. M. Taylor, D. B. Phillips, *Nat. Commun.* **2019**, *10*, 1.
[172] F. M. Mwania, M. Maringa, J. Nsengimana, *Polym. Test.* **2023**, *121*, 107981.
[173] J. P. Lewicki, J. N. Rodriguez, C. Zhu, M. A. Worsley, A. S. Wu, Y. Kanarska, J. D. Horn, E. B. Duoss, J. M. Ortega, W. Elmer, R. Hensleigh, R. A. Fellini, M. J. King, *Sci. Rep.* **2017**, *7*, 43401.
[174] L. Thijs, F. Verhaeghe, T. Craeghs, J. V. Humbeeck, J. P. Kruth, *Acta Mater.* **2010**, *58*, 9.

Nadira Meethale Palakkool completed her undergraduate degree (B.Sc) in Polymer Chemistry from Kannur University, Kerala, India in 2018. She received her MSc degree in Hydrochemistry from Cochin University of Science and Technology, Kerala, India in 2020. Now she is a Ph.D. student at the Department of Mathematics, Physics and Electrical Engineering of Northumbria University, Newcastle. Her research is focused on developing novel 3D-printed electrodes for water splitting.

Mike P. C. Taverne received an engineering degree from Télécom Physique Strasbourg, Strasbourg, France in 2007 and an M.Sc degree in subatomic physics and astroparticles from Louis Pasteur University, Strasbourg, France in 2008. He later completed a Ph.D. in the Dept. of Electrical and Electronic Engineering at the University of Bristol, UK in 2017. Now he is a Research Fellow in the Department of Mathematics, Physics, and Electrical Engineering at Northumbria University. His research interests lie primarily in the fields of quantum optics, nanophotonics, nanomanufacturing techniques, and computational photonics.

Owen Bell completed his B.Sc in Electrical Engineering at Northumbria University, UK, in 2024. Currently, he is pursuing a Ph.D. in the Department of Mathematics, Physics, and Electrical Engineering at Northumbria University. His research focuses on engineering hyperuniform disordered architectures to enhance thermal absorption.

Jonathan D. Mar is a senior lecturer in Physics in the School of Mathematics, Statistics, and Physics at Newcastle University. Prior to this, he was a research scientist at the Hitachi Cambridge Laboratory and a junior research fellow at St. Edmund's College, Cambridge University. As a commonwealth trust scholar, he obtained a Ph.D. in Physics from St. John's College, Cambridge University, following a B.A.Sc. in Electrical Engineering from the University of Toronto, Canada. His research has been supported by more than £3M from various funding bodies including the EPSRC and The Royal Society.

Vincent Barrioz, a professor in the Department of Mathematics, Physics, and Electrical Engineering. He earned his Ph.D. from the University of Wales in 2002, funded by Thales Optics, focusing on a laser-fiber system for in-situ stress monitoring of thin films. Over the past 20 years, he has specialized in photonic structures and photovoltaic devices, developing key layers for CdTe solar cells with 15% efficiency using a patented all-MOCVD process. Collaborating with Scanwel Ltd., we patented a high throughput inline chamber-less design. As part of the LCRI, he explored renewable energy solutions for residential and commercial use.

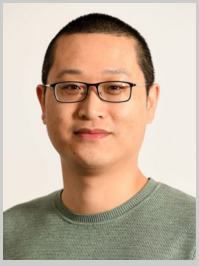

Yongtao Qu, an associate professor in Physics, focuses on developing light-absorbing layers for clean electricity generation. He has published over 30 research articles in top journals like progress in photovoltaics and composites part A. Dr. Qu led a £247k British Council-Newton Fund project on ultralight absorbers and hosted a £135k Royal Society-Newton Fellowship on lightweight PVs for IoT. He secured a €2.67M Horizon Europe MSCA grant for 6G sensor networks. Dr. Qu has given 10+ talks, organized 5+ events, reviewed for 10+ journals, and serves as an associate editor for Frontiers in Chemistry.

Chung-Che Huang earned his Ph.D. from the University of Southampton in 2005. Since 2001, he has focused on functional chalcogenide materials using CVD, ALD, and Van der Waals Epitaxy. His work includes fabricating wafer-scale 2D materials like graphene and MoS_2, with significant impact in the research community. He has over 60 academic collaborations and more than 80 publications, including 13 invited talks. He holds a patent on germanium sulfide materials. Currently a Senior Research Fellow at ORC, he leads research on advanced chalcogenide and 2D materials, contributing to EPSRC grants exceeding £21M.

Ying-Lung Daniel Ho, an associate professor of Nanophotonics and Electrical Engineering, he joined Northumbria University in 2019. He holds a B.Sc from National Taipei University of Technology and a Ph.D. from the University of Bristol. His Nanophotonic Engineering Laboratory focuses on artificially structured materials, characteristics, and micro/nano-fabrication. These efforts advance applications in nanophotonics, optoelectronics, energy storage, and quantum technologies. Current EPSRC-funded projects involve 3D nanophotonics, smart stent monitoring for coronary artery restenosis, and hyperuniform disordered metasurfaces.